ACS OMEGA

Open Access

http://pubs.acs.org/journal/acsodf

Article

ROS-responsive MSC-derived Exosome Mimetics Carrying MHY1485 Alleviate Renal Ischemia Reperfusion Injury through Multiple Mechanisms

Zhiyu Qian,[⊥] Xinyue Zhang,[⊥] Jiahua Huang, Xinhao Niu, Cuisong Zhu, Zongguang Tai, Quangang Zhu, Zhongjian Chen, Tongyu Zhu,* and Guoyi Wu*

Cite This: *ACS Omega* 2024, 9, 24853−24863

Read Online

ACCESS | Metrics & More | Article Recommendations

ABSTRACT: Renal ischemia reperfusion (IR) injury is a prevalent inflammatory nephropathy in surgeries such as renal transplantation or partial nephrectomy, damaging renal function through inducing inflammation and cell death in renal tubules. Mesenchymal stromal/stem cell (MSC)-based therapies, common treatments to attenuate inflammation in IR diseases, fail to exhibit satisfying effects on cell death in renal IR. In this study, we prepared MSC-derived exosome mimetics (EMs) carrying the mammalian target of the rapamycin (mTOR) agonist to protect kidneys in proinflammatory environments under IR conditions. The thioketal-modified EMs carried the mTOR agonist and bioactive molecules in MSCs and responsively released them in kidney IR areas. MSC-derived EMs and mTOR agonists protected kidneys synergistically from IR through alleviating inflammation, apoptosis, and ferroptosis. The current study indicates that MSC-TK-MHY1485 EMs (MTM-EM) are promising therapeutic biomaterials for renal IR injury.

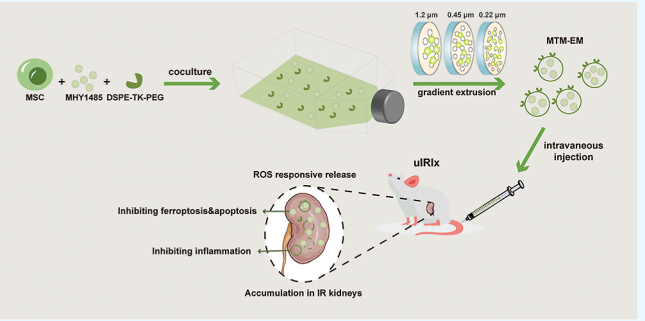

1. INTRODUCTION

Renal IR injury is a common kidney injury that acts as a result of a transient reduction of blood flow to the kidney, followed by blood reperfusion.[1] It occurs commonly in renal surgery, cardiac surgery, and kidney transplantation.[2] For renal and cardiac surgery, renal IR injury may cause acute kidney injury, chronic kidney disease, and renal fibrosis.[3] For renal transplantation, renal IR injury is inevitable and associated with rejection, delayed graft function, and transplanted kidney failure.[3,4] In recent years, an increasing number of studies have shown that both ischemia and reperfusion induce renal injury through several mechanisms, such as the generation of reactive oxygen species (ROS), renal inflammation, and the induction of renal cell death.[5] IR-induced kidney injury involves multiple death modalities of various cell types, among which apoptosis and ferroptosis of renal tubular cells are predominant.[5−7] Therefore, inhibiting inflammation, apoptosis, and ferroptosis in renal tubular cells is a potential target in renal IR treatment.

The activation of the mammalian target of rapamycin under IR conditions can mitigate IR injury through attenuating ferroptosis and apoptosis via the downregulation of autophagy.[8−11] mTOR is an evolutionarily conserved serine/threonine protein kinase that regulates multiple cellular processes. mTORC1, one of the functional complexes formed by activated mTOR, plays essential roles in the regulation of cell metabolism, mitochondrial biogenesis, and autophagy.[12] However, mTORC1 can be suppressed by hypoxia and energy stress, both of which are frequently observed under conditions of IR. Under such conditions, suppressed mTORC1 is known to activate autophagy, apoptosis, and ferroptosis while inhibiting protein biosynthesis, cell growth, and cell cycle progression.[13,14] 4,6-dimorpholino-*N*-(4-nitrophenyl)-1,3,5-triazin-2-amine (MHY1485), an mTOR agonist, alleviates the pathophysiological changes induced by downregulated mTORC1, but few studies have been conducted to explore its role in IR diseases.[15] Thus, we focused on the attenuating effects of MHY1485 on renal IR injury.

To improve the therapeutic effects and minimize the side effects of MHY1485 in the treatment of renal IR injury, MSC-derived exosome mimetics were adopted to deliver MHY1485 to IR kidneys. Mesenchymal stromal/stem cells have been the hotspot of organ repair research, considering their potential to

Received: February 20, 2024
Revised: April 22, 2024
Accepted: April 25, 2024
Published: May 28, 2024

differentiate into a variety of mesenchymal tissue lineages.[16,17] MSCs themselves and their exosomes, two common therapies in organ protection and regeneration, are able to alleviate inflammation and organ injury in IR-related diseases through stimulating tissue regeneration, inhibiting immunological responses, and blocking ROS production.[17] However, the side effects of intravenously injection of MSCs[18,19] and low yields of MSC exosomes[20,21] hampered their clinical practice. Herein, we adopted a novel approach to producing MSC-derived EMs through performing gradient extrusion on MSCs with polycarbonate membranes. The MSC-derived EMs retained the capabilities mentioned above with the exclusive advantages of fewer side effects than intravenous injection of MSCs and better productivity and purity than exosomes.[22−24] Furthermore, to enable the EMs to release contents in IR kidneys, we embedded ROS-sensitive lipids thioketal (TK) into the MSC membrane, considering the high ROS level in IR kidneys.[25]

Therefore, we established MTM-EM to mitigate renal IR injury. The MSC membrane and the TK, respectively, enabled the EM to target IR kidneys and release drugs ROS-responsively. The bioactive molecules in MSCs and the mTOR agonist improved renal function and attenuated cell death in kidneys, especially for renal tubular cells. This study explored the potential of mTOR agonists in IR-related diseases and confirmed their synergism with MSC-derived EMs to mitigate IR injury and improve the function of organs through the inhibition of inflammation, apoptosis, and ferroptosis.

2. RESULTS

2.1. Preparation and Characterization of MTM-EM. To determine the optimal concentration of MHY1485 and MSC protein for TCMK-1 cells, we tested the effects of coincubation with different concentrations of MHY1485 and MSC protein for 24 h on TCMK-1 cell viability. The results showed that 5 μg/mL MHY1485 or 0.5 mg/mL MSC protein did not exhibit toxicity on TCMK-1 cells (Figure 1A,B). Therefore, we chose MHY1485 at 5 μg/mL concentration and MSC protein at 0.5 mg/mL concentration as the components of MTM-EM.

A UV spectrophotometer was used to determine the encapsulation efficiency of MHY1485 in MTM-EM. Based on the significant absorption of MHY1485 at 250 nm (Figure 1C), we established a standard curve for the concentration-OD value of MHY1485 at this wavelength (Figure 1D), and the encapsulation efficiency of MHY1485 in MTM-EM was 11.768 ± 0.252%. Considering the encapsulation efficiency and the optimal concentration of MHY1485 and MSC protein for TCMK-1, we adjusted the concentration of MSC protein and MHY1485 to ensure the optimal benefits of MTM-EM for TCMK-1 cells.

Transmission electron microscope (TEM) images revealed that MTM-EM and MSC-TK EMs (MT-EM) were of vacuolar shape with a membrane structure. MTM-EM exhibited a size of approximately 271.73 ± 19.12 nm with a uniform distribution (Figure 1E), while the size of MT-EM was 250.23 ± 6.41 nm. Additionally, the drug release rate of MTM-EM in high ROS-level environments was significantly higher than that under normal conditions (Figure 1F), confirming the effect of TK on ROS-responsive drug release.

2.2. Uptake and Therapeutic Effects of MTM-EM. Next, we examined the uptake of MTM-EM by TCMK-1. To visualize the uptake, we labeled MTM-EM with DiD red fluorescent dye. The uptake of MTM-EM exhibited a time-dependent pattern (Figure 2A), reaching its maximal fluorescence intensity after 4 h of coincubation, with no subsequent increase observed. Thus, we determined 4 h as the optimal duration for TCMK-1 cells to internalize MTM-EM.

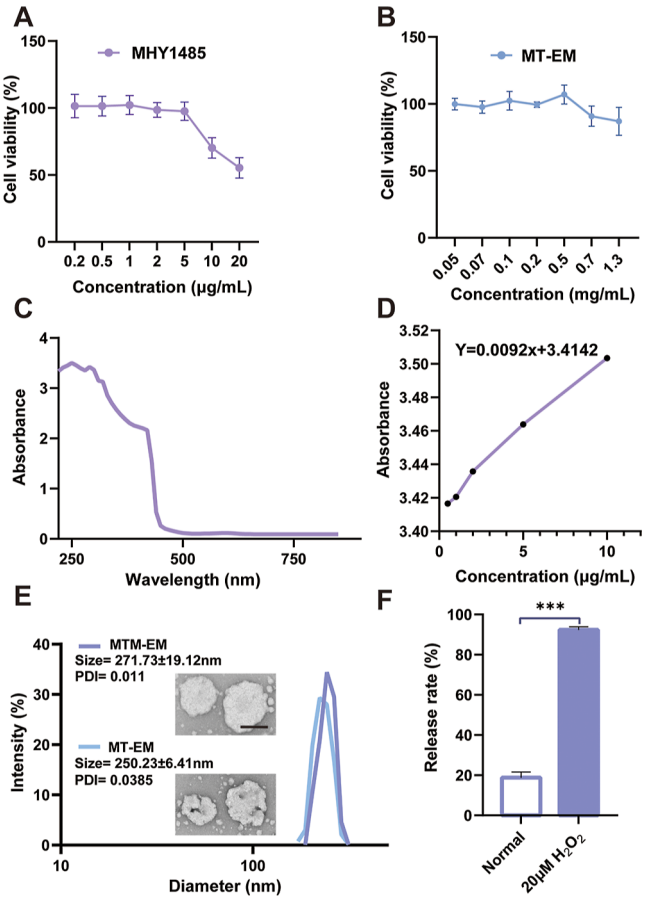

Figure 1. Characterization of MTM-EM. (A) Cell viability of TCMK-1 treated with different concentrations of MHY1485. (B) Cell viability of TCMK-1 treated with different concentrations of MT-EM. (C) Ultraviolet−visible absorption spectra of the MHY1485. (D) Standard curve detecting MHY1485 in MTM-EM using a ultraviolet spectrophotometer. (E) Size distribution, PDI, and TEM images of MTM-EM and MT-EM. Scale bar: 200 nm. (F) Release rate of MHY1485 from MTM-EM (0.5 mg/mL) under normal and high ROS conditions. All data are shown as the mean ± SD (n = 3). ***P < 0.001; t-test.

A confocal microscope was also used to observe the cellular uptake. MTM-EM@DiD emitted red fluorescence, while lysosomes dyed with LysoTracker Green emitted green fluorescence (Figure 2B). The red fluorescence around the nucleus suggested that MTM-EM had been internalized by cells, confirming the successful uptake. Notably, some of the red fluorescence did not overlap with green lysosomes, indicating that MTM-EM partially escaped the degradation of lysosomes,[26] further confirming the effective utilization of MTM-EM by TCMK-1.[27]

To investigate the efficacy of MTM-EM on the cell viability of renal tubular cells under IR, we established the IR TCMK-1 model based on previous studies.[2,61] The CCK-8 result showed that IR decreased the cell viability of TCMK-1 cells to 44.59 ± 3.45% (Figure 2C). Treatment with MT-EM or MHY1485 mitigated the loss of IR-induced cell viability significantly, and MTM-EM (81.08 ± 3.15%) showed better pharmaceutic

https://doi.org/10.1021/acsomega.4c01624
ACS Omega 2024, 9, 24853−24863

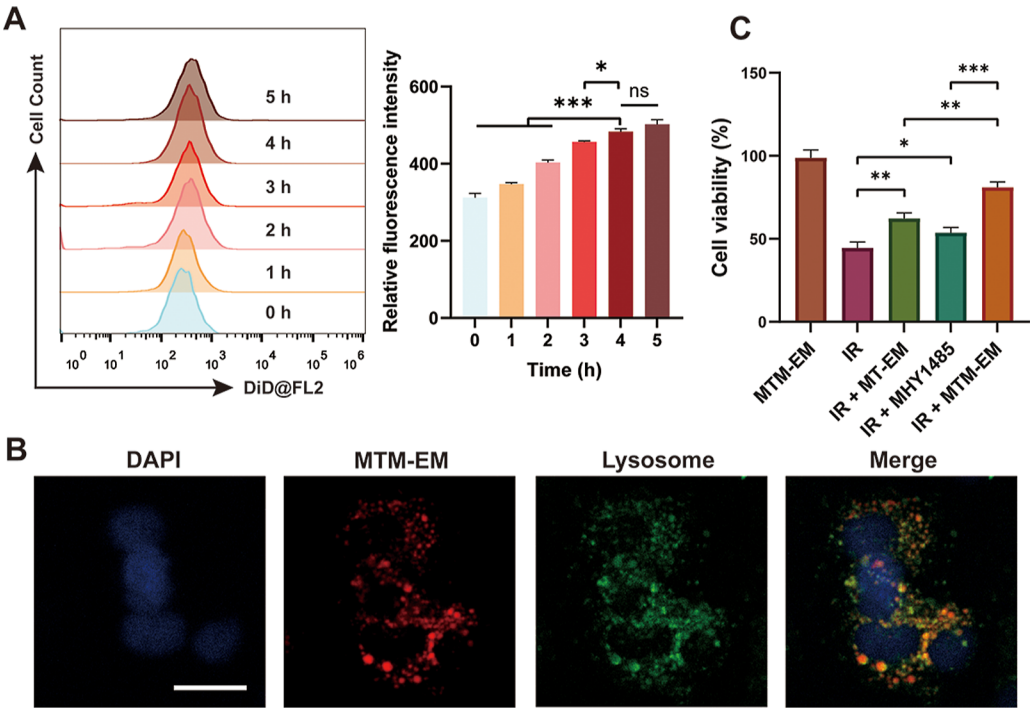

Figure 2. Uptake of MTM-EM by TCMK-1 and its effect on cell viability. (A) Cellular uptake of MTM-EM detected by flow cytometry and its statistical analysis. (B) Confocal microscope images of MTM-EM@DiD after coincubation with TCMK-1. Scale bar: 25 μm. (C) Cell viability of TCMK-1 under corresponding treatments measured by the CCK-8 assay. All data are shown as the mean ± SD (n = 3). ns: not significant, *P < 0.05, **P < 0.01, ***P < 0.001; t-test.

efficacy than MT-EM or MHY1485. Compared with the control group, the MTM-EM group showed no significant difference in cell viability, confirming the low toxicity of MTM-EM. These results demonstrated that MT-EM and MHY1485 had a synergistic effect on protecting renal tubular cells from IR injury, suggesting that they might prevent IR injury in different mechanisms.

Taken together, these results confirmed the uptake of MTM-EM by TCMK-1 cells, and the optimal uptake was reached at 4 h. Additionally, the nanodelivery drug system exhibited biocompatibility and the capability to protect renal tubular cells from IR injury.

2.3. MTM-EM Alleviated In Vitro Renal IR Injury through the Inhibition of Inflammation, Apoptosis, and Ferroptosis. Next, we tried to investigate the underlying mechanism by which MTM-EM alleviated renal IR injury. IR-induced kidney injury is characterized by enhanced inflammatory responses and tubular cell death, including apoptosis and ferroptosis majorly.[28] Therefore, we focused on the effects of MTM-EM on inflammation, apoptosis, and ferroptosis.

Changes in the production of cytokines, such as TNF-α, IL-1β, and IL-6, are important features of the IR-induced renal inflammation.[29] TNF-α exhibits immune-regulatory and pro-inflammatory effects in diverse tissues, including the kidney;[30] IL-1β-dependent signaling drives renal damage and fibrosis by activating inflammation and proliferation; IL-6 is a key regulator of inflammation, regeneration, and repair in kidney.[31] The contents of TNF-α, IL-1β, and IL-6 were significantly elevated in TCMK-1 after IR (Figure 3A−C). MHY1485 did not affect the cytokine levels, whereas MT-EM and MTM-EM significantly decreased their content in TCMK-1, suggesting that MT-EM and MTM-EM had a significant inhibitory effect on the production of pro-inflammatory cytokines induced by IR, and the effect is attributed to MT-EM but not MHY1485.

The apoptosis of renal tubular cells was detected through flow cytometry. Apoptotic cells (including early apoptosis and late apoptosis) were increased after IR, which is alleviated by coincubation with MT-EM or MHY1485 (Figure 3D). Remarkably, cells treated with MTM-EM exhibited a lower apoptotic rate. Furthermore, we detected mTORC1 activity to confirm the function of MHY1485. The phosphorylation of mTOR is necessary for mTORC1 activation, which is found to regulate apoptosis and ferroptosis under IR conditions,[32] and the phosphorylation of S6 ribosomal protein reflects mTORC1 activation.[33] The immunoblotting result demonstrated that mTORC1 was inhibited during IR, while MHY1485 remarkably restored mTORC1 activity, which is further enhanced by the EM. These results indicated that MHY1485-induced mTORC1 activation and MT-EM synergistically alleviated IR-induced apoptosis of renal tubular cells.

The ferroptosis of renal tubular cells was measured by glutathione peroxidase-4 (GPx4) expression, oxidative stress, and lipid peroxide. GPx4, an important protein resisting lipid peroxidation,[34] is a crucial inhibitor and indicator for ferroptosis.[35] Compared with the cells of the control group, the expression of GPx4 was decreased in the IR model group, confirming that ferroptosis was induced under IR conditions (Figure 3E). MT-EM did not affect the GPx4 expression, while MHY1485 elevated the GPx4 expression. Additionally, cells coincubated with MTM-EM expressed more GPx4 than those coincubated with MHY1485, demonstrating the stronger inhibitory effect of MTM-EM on ferroptosis than MHY1485.

Since ferroptosis is also characterized by oxidative stress, biochemical tests of superoxide dismutase (SOD), glutathione/glutathione disulfide (GSH/GSSG), and malondialde-

https://doi.org/10.1021/acsomega.4c01624
ACS Omega 2024, 9, 24853−24863

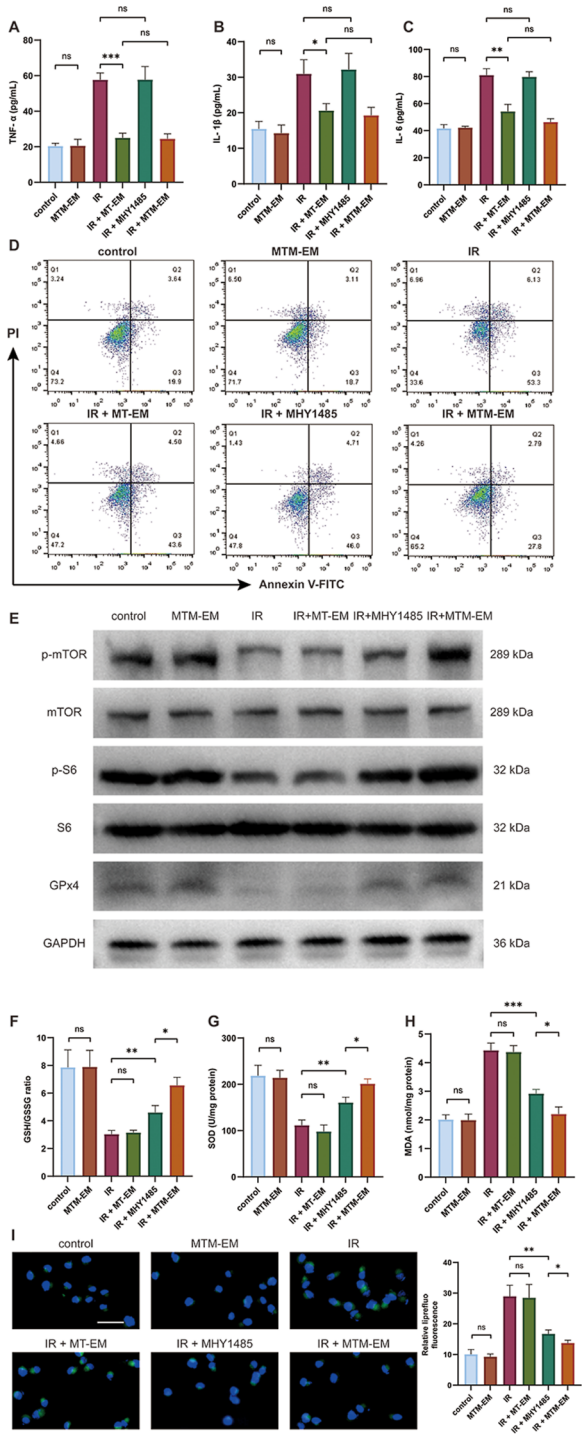

Figure 3. Mechanisms by which MTM-EM alleviated IR-induced cell death. (A–C) Levels of TNF-α (A), IL-1β (B), and IL-6 (C) in TCMK-1 cells with corresponding treatment detected by enzyme-linked immunosorbent assay (ELISA). (D) Apoptosis assay of TCMK-1 cells with corresponding treatment detected using flow cytometry. (E) GPx4 protein levels and phosphorylation of mTOR and S6 ribosomal proteins in TCMK-1 cells, as detected by Western blot. (F–H) GSH/GSSG (F), SOD (G), and MDA (H) levels in TCMK-1 cells detected by biochemical tests. (I) Cellular lipid peroxides of TCMK-1 cells detected by liperfluo and its statistical analysis. Scale bar: 50 μm. All data are shown as the mean ± SD (n = 3). ns: not significant, *P < 0.05, **P < 0.01, ***P < 0.001; t-test.

hyde (MDA) were performed. SOD plays a primary role in the cellular defense against an oxidative insult by ROS;[36] GSH is necessary for the activation of GPx4, and GSH/GSSG reflects the GSH activity;[37,38] MDA is one of the prominent byproducts of lipid peroxidation.[39] The biochemical results demonstrated that MHY1485 could relieve the IR-induced increase of ROS production and impairment of ROS defense system, and MTM-EM exhibited stronger efficacy (Figure 3F–H).

"Liperfluo" is a fluorescence dye detecting lipid peroxides, which is a characteristic substance in ferroptosis.[40] Compared with the control group, cells contained much more lipid peroxides after IR treatment, with or without coincubation with MT-EM (Figure 3I). MHY1485 significantly decreased the fluorescence, and MTM-EM further alleviated the production of lipid peroxides. These results demonstrated that MHY1485-induced mTOR activation alleviated IR-induced ferroptosis in renal tubular cells, and the EM drug delivery system could augment the efficacy.

Altogether, MTM-EM alleviated cell death and promoted cell viability through the mitigation of inflammation, apoptosis, and ferroptosis.

2.4. MTM-EM Alleviated Kidney Injury of uIRIx Mice.

Before testing the therapeutic efficacy of MTM-EM on IR kidneys, we first detected the safety of MTM-EM in vivo. MTM-EM did not affect the structure of major organs, as shown by the H&E staining of the heart, liver, lung, spleen, and kidney (Figure 4A). Compared with mice in the control group, mice administered with MT-EM, MHY1485, or MTM-EM had similar serum AST, ALT, creatinine, and urea nitrogen (Figure 4B,C), confirming that MTM-EM did not damage the main organs morphologically or functionally, indicating the in vivo safety of MTM-EM.

Then, we examined the in vivo distribution of MTM-EM. We established MTM-EM/DiR through dyeing MTM-EM with DiR, a common near-infrared dye for cell membranes. Then, MTM-EM@DiR were intravenously injected into sham mice or IR mice, and their distribution in the kidneys was detected at 1, 12, and 24 h after injection. The MTM-EM@DiR did not accumulate in sham kidneys at any time point. Comparatively, the amount of MTM-EM@DiR was apparently increased at 12 h, and the accumulation further increased at 24 h (Figure 4D), demonstrating that MTM-EM targeted the IR-treated kidney. Their excellent targeting effect ensured their effect on kidney protection. The targeting of MTM-EM might be attributed to the chemotaxis of MSCs to inflammatory and high ROS-level areas.[41]

To examine the effect of nanoparticles on renal IR injury in vivo, we then established the unilateral IR injury with contralateral nephrectomy (uIRIx) in mice based on previous studies.[2,62] The Scr and BUN levels elevated to 167.70 ± 11.77 μmol/L and 77.93 ± 5.63 mmol/L in the IR mouse kidneys (Figure 4E). After treatment with MT-EM or MHY1485, the Scr was 87.95 ± 6.35 and 91.37 ± 9.59 μmol/L, respectively, and the BUN level was 29.60 ± 6.30 and 29.51 ± 5.04 mmol/L, respectively, indicating that MT-EM and MHY1485 mitigated the IR injury of kidneys. Importantly, mice treated with MTM-EM exhibited lower Scr (47.66 ± 6.10 μmol/L) and BUN (17.51 ± 3.45 mmol/L) levels.

PAS staining is widely used to observe the morphology of renal tubules.[42] The PAS staining image of uIRIx kidneys treated with Phosphate buffer solution (PBS) showed necrotic renal tubules, tubular distension, and a loss of brush border

https://doi.org/10.1021/acsomega.4c01624
ACS Omega 2024, 9, 24853–24863

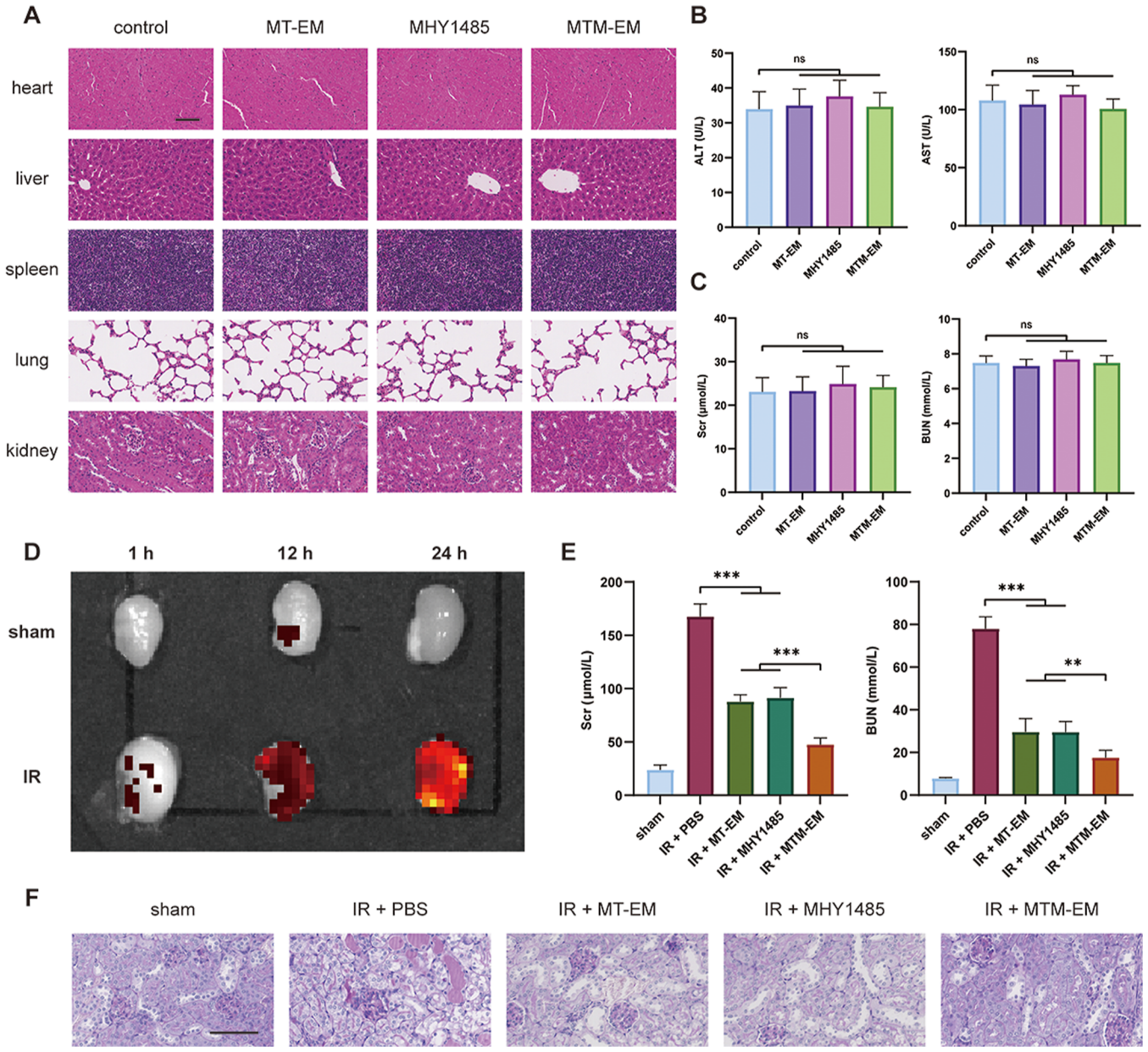

Figure 4. In vivo safety, targeting, and efficacy of MTM-EM on IR kidneys. (A) H&E staining of the heart, liver, spleen, lung, and kidney in mice treated by indicated drugs. Scale bar: 50 μm. (B,C) Liver function (B) and kidney function (C) of mice treated by indicated drugs. (D) Relative accumulation of MTM-EM@DiR at 1, 12, or 24 h after injection in mouse kidneys with or without ischemia reperfusion. (E) Effects of MTM-EM on IR-induced renal dysfunction detected using biochemical tests. (F) Effects of MTM-EM on IR-induced renal morphological abnormalities detected by PAS staining. Scale bar: 50 μm. All data are shown as the mean ± SD (n = 5). ns: not significant, $^{**}P < 0.01$, $^{***}P < 0.001$; t-test.

membranes (Figure 4F). In the MT-EM or MHY1485 group, renal tubular necrosis was completely inhibited, and the change of brush border membranes and tubular distension was alleviated compared with that in the PBS IR group. After treatment with MTM-EM, renal tubular dilation and the loss of brush border membranes were further alleviated.

Altogether, these results demonstrated that MTM-EM could improve renal IR injury and kidney function with satisfying safety and targeting.

2.5. MTM-EM Inhibited Inflammation, Apoptosis, and Ferroptosis in uIRIx Mouse Kidneys. After confirming the protecting efficacy of MTM-EM on IR kidneys in vivo, we tried to determine the underlying mechanisms. First, we detected the IR-related inflammatory cytokines. The contents of TNF-α, IL-1β, and IL-6 in uIRIx kidneys were significantly higher than those in sham kidneys, indicating that the inflammatory response was highly activated in uIRIx kidneys (Figure 5A–C). Administering MT-EM or MTM-EM decreased TNF-α, IL-1β, and IL-6 level in uIRIx kidneys, while MHY1485 did not exhibit the inhibitory effect. These findings demonstrated the effect of MTM-EM on the mitigation of inflammation in uIRIx kidneys.

Then, we examined the apoptosis in uIRIx kidneys harvested from mice by immunohistochemistry (IHC) staining of cleaved caspase 3(Figure 5D), a vital protein and indicator in the process of apoptosis.[43] The uIRIx kidneys in the PBS group showed a significant increase in cleaved caspase 3 positive areas, confirming the IR-induced apoptosis. MT-EM

https://doi.org/10.1021/acsomega.4c01624
ACS Omega 2024, 9, 24853−24863

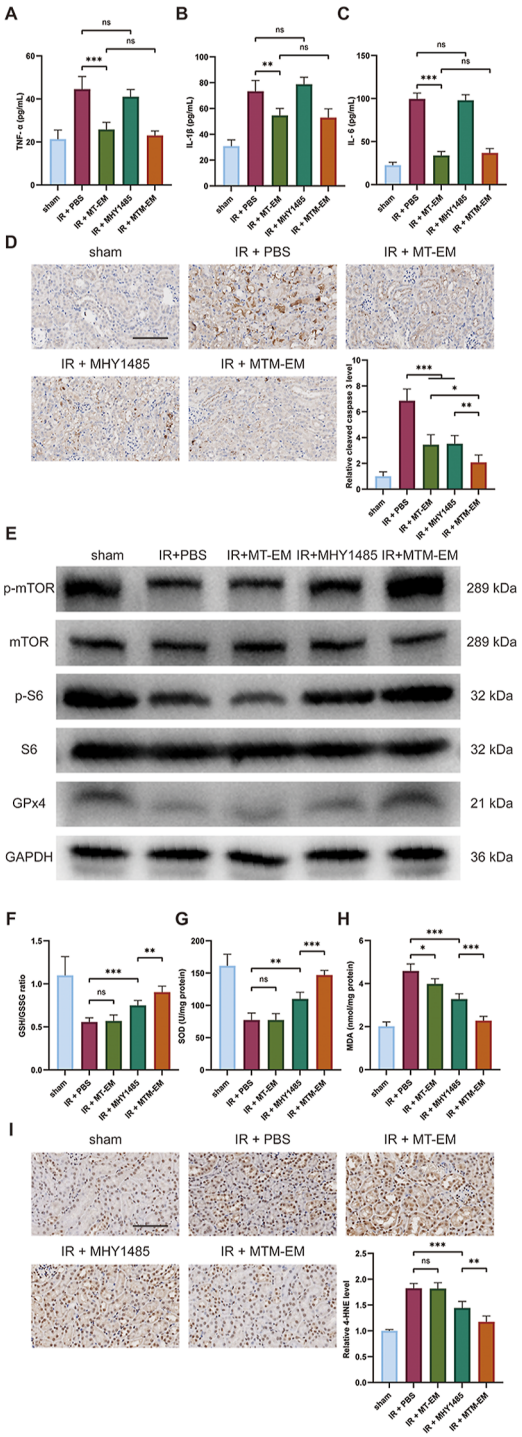

Figure 5. Mechanisms by which MTM-EM alleviated IR-induced mouse renal injury. (A−C) Levels of TNF-α (A), IL-1β (B), and IL-6 (C) in mouse kidneys detected by ELISA. (D) Relative cleaved caspase 3 levels in mouse kidneys detected by IHC and its statistical analysis. Scale bar: 50 μm. (E) GPx4 protein levels and phosphorylation of mTOR and S6 ribosomal protein in mouse kidneys, as detected by Western blot. (F−H) GSH/GSSG (F), SOD (G), and MDA (H) levels in mouse kidneys detected by biochemical tests. (I) Lipid peroxides in mouse kidneys detected by IHC staining of 4-HNE and the statistical analysis. Scale bar: 50 μm. All data are shown as the mean ± SD (n = 5). ns: not significant, *P < 0.05, **P < 0.01, ***P < 0.001; t-test.

or MHY1485 reduced the number of positive cells significantly, whereas the fewest cleaved caspase 3 positive areas were observed in the MTM-EM group. The immunoblotting result also demonstrated that MHY1485 alleviated the IR-induced mTORC1 dysfunction, which could be further promoted by MTM-EM. These findings suggested that both MT-EM and MHY1485-induced mTORC1 activation were effective in attenuating renal cell apoptosis induced by IR injury, and they synergized on protecting renal cells from IR-induced apoptosis.

Next, we examined the inhibitory effects of MTM-EM on IR-induced ferroptosis. The GPx4 expression was much lower after IR (Figure 5E). MT-EM did not affect GPx4 expression, but MHY1485 increased the GPx4 level, and mice with MTM-EM treatment expressed more GPx4 in kidneys than those with MHY1485 treatment, indicating that MHY1485 inhibited ferroptosis in uIRIx kidneys, which could be enhanced by the EMs. The biochemical tests (Figure 5F−H) and IHC of 4-HNE (Figure 5I) were used to detect the oxidative stress status and lipid peroxides, respectively. Mouse uIRIx kidneys treated by PBS or MT-EM showed significant oxidative stress and lipid peroxide production, which was mitigated by MHY1485. MTM-EM further improved the protective effect. These results suggested that MHY1485 alleviated ferroptosis effectively. Although MT-EM alone did not influence ferroptosis, the drug delivery system could improve the efficacy of MHY1485, which might be attributed to the accurate delivery and release of drugs in kidneys.

Taken together, these results suggested that MTM-EM mitigated renal IR injury and preserved renal function through attenuating inflammation, apoptosis, and ferroptosis in IR mouse kidneys.

3. DISCUSSION

Kidney IR injury is common in renal surgery and results in acute kidney injury, chronic kidney disease, and kidney fibrosis, eventually inducing kidney dysfunction. Recent studies have revealed that the renal IR injury was mediated by activated inflammation, apoptosis, and ferroptosis.[44] MSC therapy is widely studied due to its ability to reduce inflammation in IR areas. However, the efficacy of MSC therapy on IR-related diseases in clinical research is unsatisfactory, partially because it cannot effectively inhibit cell death such as ferroptosis and apoptosis.[45] To address these clinical challenges, we prepared the therapeutic biomaterial MTM-EM to protect kidneys from IR injury. MHY1485 in MTM-EM targeted the mTOR pathway and alleviated apoptosis and ferroptosis. Meanwhile, the MSC-derived EMs improved the biocompatibility and efficacy of MHY1485 and maintained the functions of MSCs, including targeting IR kidneys and inhibiting inflammation. Additionally, the MTM-EM were reasonably designed to be ROS-responsive, which promoted accurate drug release in the IR kidneys. In this study, the MTM-EM exhibited attenuating effects on IR-induced kidney injury.

MSCs and their exosomes were widely used to treat kidney diseases and showed inhibitory effects on apoptosis and inflammation. However, the MSC-based cell therapy exhibited potential side effects such as tumor formation, immune response, and embolism. Meanwhile, the majority of MSCs injected into bodies would be trapped in the lungs, limiting their function in injured kidneys. Traditional extraction methods of MSC exosomes resulted in their low yields and reduced purity.[46] In the current study, the gradient extrusion

https://doi.org/10.1021/acsomega.4c01624
ACS Omega 2024, 9, 24853−24863

was performed to produce MSC-derived EMs to overcome such disadvantages of cell therapy or exosomes. Since targeting IR tissues is one of the advantages of MSC therapy, our study confirmed that MTM-EM accumulated in IR kidneys but not in sham kidneys, demonstrating that EM maintained the excellent targeting ability of MSCs. This is possibly because MTM-EM retain the lipid composition and surface molecules of MSCs, which allow MTM-EM to localize automaticlly to IR kidney tissues.[47,48] Additionally, TK was embedded in the membrane to enhance the therapeutic effects through improving the release of mTOR agonists and bioactive molecules in the IR environment.

IR injury is an inflammation-related disease. The sterile inflammation induced by IR is characterized by the production of cytokines, chemokines, and other pro-inflammatory stimuli. TNF-α, a major contributor to the pathogenesis of IR in most tissues produced by a variety of cell types, induces the expression of chemokines and the production of ROS, promoting the recruitment and activation of immune cells in IR kidneys.[49] IR-induced damage-associated molecular patterns and TNF-α enhance the expression of IL-1β and IL-6, upregulating adhesion molecules and promoting lymphocyte recruitment in IR areas.[50] The miRNAs in MTM-EM, such as miR-1184 and miR-146b, are found to decrease the secretion of pro-inflammatory cytokines through regulation on NF-κB, Sirtuin-1, or IL-1 receptor-associated kinase signaling pathways, eventually mitigating immune responses in IR kidneys.[51−53]

Apoptosis is a prevalent and important regulated cell death mode in IR.[48] The activation of Fas, TNF-α, and TNF-related apoptosis-inducing ligand receptors induced by IR recruits a number of death domain-containing proteins, ultimately cleaving and activating caspase-3.[54] This study demonstrated that MT-EM and MHY1485 synergistically inhibited apoptosis. The MT-EM can also protect kidneys from apoptosis through specific miRNAs. For example, miR-199a-3p and miR-199a-5p in MSCs can activate pathways, including the AKT or ERK pathway, promoting tubular cell proliferation and limiting apoptosis during kidney IR, eventually leading to the amelioration of the loss of kidney function.[55,56]

mTOR is a sensor for energy and metabolism status and plays an integral role in regulating apoptosis. Phosphatidylinositol-3-kinase/Akt/mTOR is a classic apoptosis regulatory pathway which downregulates apoptosis in an autophagy-dependent mechanism.[57] However, under IR conditions, mTORC1 is strongly inhibited, leading to subsequent activation of apoptosis, which resembles the phenomenon under treatment with mTOR inhibitors. MHY1485 could reverse the IR-induced downregulation of mTOR activity, inhibiting autophagy and alleviating apoptosis. MT-EM and MHY1485 inhibited apoptosis through different pathways, enabling MTM-EM to exhibit synergistic effects on mitigating apoptosis.

Ferroptosis is characterized by the iron-dependent accumulation of reactive lipid peroxides[58] and is one of the most prominent forms of cell death under IR conditions. In the ischemic phase, nuclear receptor coactivator 4-mediated ferritinophagy, one of the most closely related types of autophagy to ferroptosis, is activated, leading to ferroptosis by degrading ferritin and inducing iron overload.[59] During reperfusion, the rapid restoration of nutrients induces a burst of ROS production and ferroptosis.[60] In this current study, MHY1485 directly activated mTORC1, and the activated mTORC1 could inhibit autophagy, including ferritinophagy. As a result, ferritin was restored, iron overload and ferroptosis were alleviated, and renal function was improved.

The current MSC-derived drug delivery system maintains the therapeutic effects of MSCs on renal IR while improving the biocompatibility and effects of MHY1485. The drug delivery system and MHY1485 synergistically alleviated renal IR injury. This current study provides a novel approach, other than cell therapy and exosome-based therapy, for the application of MSC-based therapies to kidney IR. Furthermore, this MSC-derived drug delivery system has the potential to be pretreated or modified to express specific proteins or carry other small molecule drugs for different pathophysiological situations.

4. CONCLUSIONS

In this current study, we developed TK-modified MSC-derived EMs carrying MHY1485 to protect kidneys from IR injury. MTM-EM maintained the function of MSCs and improved the biocompatibility of MHY1485. The MSC-derived EMs and MHY1485 exhibited synergistic protective effects on renal morphology and function, and the underlying mechanisms include the downregulation of inflammation, apoptosis, and ferroptosis.

5. MATERIALS AND METHODS

5.1. Cell Culture and the In Vitro IR Model. Transformed C3H mouse kidney-1 (TCMK-1) cells (mouse renal tubular epithelial cells) and placenta mesenchymal stromal/stem cells were purchased from FuHeng Biology (Shanghai, China) and Procell Life Technology (Wuhan, China). The cells were cultured in Dulbecco's modified Eagle medium (DMEM) (Biosharp, BL301A) supplemented with 10% fetal bovine serum (LONSA; S711-001S).

The in vitro IR model was established based on previous studies.[2,61] Briefly, TCMK-1 cells were washed, cultured in glucose-free DMEM (Biosharp, BL1125A) without fetal bovine serum, and exposed to hypoxia. Hypoxia was introduced by using a hypoxia chamber along with a compact gas controller that controls oxygen concentration at 1%, achieved by administering 95% nitrogen and 5% carbon dioxide. The ischemia period lasts 12 h, following a reperfusion period of 6 h. During the reperfusion period, TCMK-1 cells were cultured under normal conditions.

5.2. Animal Models and Animal Experiment Statement. All animal experiments were approved by the animal ethics committee of Fudan University (Ethical approval number: 2019-HSYY-JS-240) and conformed to the guidelines of the National Research Council for Laboratory Animal Care in Research.

Six-week-old male BALB/c mice were purchased from Shanghai JieSiJie Laboratory Animal (Shanghai, China). Mice were housed under specific pathogen-free conditions with standardized food and water and controlled temperature (21−25 °C) and humidity (40−70%).

To induce ischemia-reperfusion injury of the kidneys, we performed uIRIx models on BALB/c mice, as described in previous studies.[2,62] For sham groups, we performed unilateral nephrectomy only. PBS, drugs, or EMs were intravenously injected 4 h before surgery. 48 h after surgery, mice were sacrificed by CO_2 asphyxia, and blood samples and tissues were collected.

https://doi.org/10.1021/acsomega.4c01624
ACS Omega 2024, 9, 24853−24863

5.3. Preparation and Characterization MTM-EM. MSCs were cocultured with 50 μg/mL MHY1485 for 4 h. Then, the MHY1485-loaded MSCs were trypsinized and dispersed in PBS containing 50 μg/mL MHY1485 and 5 mg/mL 2-distearoyl-*sn*-glycero-3-phosphoethanolamine−thioketal−polyethylene glycol (DSPE−TK−PEG) (Ruixi Biotechnology, Xi'an, China). The cell suspension was extruded through a pneumatic extruder (PhD Technology LLC, St. Paul, MN, USA) prepared with 1.2 μm (RAWP04700, Merck, NJ, USA), 0.45 μm (TJMF0446, JinTeng, Tianjin, China), and 0.22 μm (TJMF0445, JinTeng) polycarbonate filters. The obtained product was centrifuged at 100,000*g* for 2.5 h and washed with PBS twice. MHY1485 was internalized by MSCs during coincubation and encapsulated in MTM-EM through the extruding process.

The MT-EM were obtained in a similar way. Briefly, MSCs were collected and dispersed in PBS containing 5 mg of DSPE−TK−PEG; then, the cell suspension was extruded with the same method described above.

The protein concentration of MTM-EM was detected by the bicinchoninic acid (BCA) Protein Assay Kit according to the manufacture's protocols. Specifically, the sample (20 μL) was added to a 96-well plate, then the wells were filled with BCA working solution (200 μL) and incubated at 37 °C for 0.5 h. The optical density (OD) of each well was detected at 562 nm by a microplate reader (Thermo Fisher Scientific, Waltham, MA, USA).

The cell lysis solution was added to the MTM-EM, and the loading of MHY1485 in the MTM-EM cell lysate was analyzed using a SpectraMax M5 microplate reader under 250 nm (Molecular Devices, Sunnyvale, CA, USA). MHY1485 was dissolved in DMSO to dilute to an appropriate concentration, which was measured by SpectraMax M5 microplate reader to detect the highest absorbance and create a standard curve at the highest absorbance.

The polymer dispersity index (PDI) and size of MTM-EM were measured by a Nano Zetasizer (Microtrac, York, PA, USA). MTM-EM was observed using a transmission electron microscope (Hitachi, Tokyo, Japan).

5.4. Cell Viability Assay and Release Assay of MTM-EM. The cell viability profiles of MHY1485 and MT-EM in TCMK-1 were assessed using established protocols. TCMK-1 cells were seeded at a density of 6×10^3 cells per well in 96-well cell culture plates and cultured overnight. Then, the cells were treated with corresponding drugs at concentrations ranging from 0.2 to 20 μg/mL (concentration of MHY1485) or 0.05 to 1.3 mg/mL (concentration of MT-EM proteins).

Then, we added CCK-8 solution (10 μL) to each well and incubated for another 1 h. The microplate reader (Thermo Fisher Scientific, Waltham, MA, USA) was used to read absorbance at 450 nm.

To determine the release of MTM-EM in different physiological environments, we added MTM-EM to DMEM medium, with or without 20 μM H_2O_2. 24 h later, the MHY1485 content in the supernatant was detected.

5.5. Uptake Assay. MTM-EM were dyed with DiD (5 μM) for 0.5 h; then, the MTM-EM@DiD were incubated with TCMK-1 cells for 0−5 h. The obtained cells were washed and detected by flow cytometry using FACSCalibur (BD Biosciences, Franklin Lakes, NJ, USA).

To observe cells more vividly, TCMK-1 cells were seeded on a Millicell EZ SLIDE 8-well glass (PEZGS0816, Merck) overnight. Then, the medium containing MTM-EM@DiD was added to wells and incubated for 4 h. The cells were subsequently stained with LysoTracker Green (Thermo Fisher Scientific). After washing, fixing, staining with 4,6-diamidino-2-phenylindole (DAPI), the obtained sample was imaged using a confocal microscope (Leica, Wetzlar, Germany).

5.6. Enzyme-Linked Immunosorbent Assay. TCMK-1 cells were lysed with 0.25% trypsin and collected, and renal tissues were ground into a homogenate using 150 mM tris buffer. Mouse tumor necrosis factor (TNF)-α, interleukin (IL)-1β, and IL-6 were detected using the Mouse IL-6 ELISA Kit (Beyotime, PI326), Mouse IL-1β ELISA Kit (Beyotime, PI301), and Mouse TNF-α ELISA Kit (Beyotime, PT512), according to standard protocols of the manufacturer.

5.7. In Vitro Apoptosis Assay. Apoptotic cells were quantified with an Annexin V-FITC Apoptosis detection kit (Beyotime, C1062S) according to manufacturer's protocols. Briefly, cells were incubated under normal or IR conditions with or without the treatment of MT-EM, MHY1485, or MTM-EM at 37 °C. Cells were harvested, resuspended in the binding buffer, and then stained with Annexin V-FITC and propidium iodide for 15 min at room temperature. The apoptotic index was immediately determined by FACSCalibur (BD Biosciences, Franklin Lakes, NJ, USA).

5.8. Western Blotting. Cells and minced tissue were extracted in cold radioimmunoprecipitation assay buffer and detected using a BCA protein assay kit (Beyotime, P0012). Equal amounts of protein were loaded in each lane, separated by SDS-polyacrylamide gel electrophoresis, and then blotted onto a polyvinylidene difluoride membrane. After blocking for 1 h, the membrane was incubated overnight with primary antibodies at 4 °C and with secondary antibodies for 1 h at room temperature. Proteins were detected using a chemiluminescence kit (NCM Biotech, P10200) with the ChemiDoc MP Imaging System (BioRad, CA, USA).

The following primary antibodies were used in Western blotting:

GAPDH (Proteintech, 10494; 1:50000), GPx4 (Proteintech, 67763; 1:1000), Phospho-mTOR (Cell Signaling Technology, 5536S; 1:1000), mTOR (Cell Signaling Technology, 2983S; 1:1000), Phospho-S6 Ribosomal protein (Proteintech, 29223-1-AP; 1:1000), and S6 Ribosomal protein (Proteintech, 80208-1-RR; 1:5000).

The following secondary antibodies were used in Western blotting:

Antirabbit IgG (Cell Signaling Technology, 7074S; 1:1000) and antimouse IgG (Cell Signaling Technology, 7076S; 1:1000).

5.9. Biochemical Assay. The levels of serum alanine amiotransferase (ALT) (Rayto, S03030), serum aspartate transaminase (AST) (Rayto, S03040), serum creatinine (Scr) (Rayto, S03076), and blood urea nitrogen (BUN) (Rayto, S03036) were tested with corresponding testing kits using an automated biochemical analyzer (Rayto, Chemray 800) according to the manufacturer's protocols. Oxidative stress status was detected using GSH/GSSG (Beyotime, S0053), MDA (Jiancheng Bioengineering, A003-1-2), and SOD (Jiancheng Bioengineering, A001-1-2) assay kits according to manufacturer's protocols.

5.10. In Vitro Lipid Peroxidation Assay. Cells were seeded into 4-well chambers and incubated with the indicated treatments in 5% CO_2 at 37 °C. During the last 30 min of incubation, 1 μg/mL Hoechst 33342 and 1 μM Liperfluo (Dojindo, L248) dyes were added. After washing with PBS

https://doi.org/10.1021/acsomega.4c01624
ACS Omega 2024, 9, 24853−24863

twice, cells were imaged using a fluorescence microscope. The relative lipid peroxidation level was quantified by the green fluorescence intensity.

5.11. IHC and Historical Staining. Kidneys and other organs were removed, fixed in 10% formalin, and embedded in paraffin. Sections were stained with hematoxylin−eosin (HE) or periodic acid-Schiff (PAS) to evaluate the histological changes. Immunohistochemical analysis was performed by using specific antibodies. After the color reaction, the images of staining were captured using a microscope (Nikon, H550S, Tokyo, Japan). The relative protein levels were quantified by the proportion of the positive area.

The following antibodies were used in IHC:

Cleaved caspase 3 (Beyotime, AC033; 1:100) and 4-HNE (Bioss, bs-6313R; 1:500).

5.12. In Vivo Distribution Assay. MTM-EM@DiR was established through dyeing MTM-EM with DiR. Then, MTM-EM@DiR was intravenously injected into sham mice or IR mice, and its contents in the kidneys were detected by IVIS Lumina K at 1, 12, and 24 h after injection.

5.13. Statistical Analysis. Data are presented as (mean ± SD), except where otherwise indicated. GraphPad Prism 9.0 (San Diego, CA, USA) was used to collect and analyze the data. An unpaired Student's *t*-test was used to compare the values of two groups. A two-tailed *P* value of <0.05 was considered statistically significant and was marked as "*", a *P* value of <0.01 was marked as "**", and a *P* value of <0.001 was marked as "***", except where otherwise indicated. No samples or animals were excluded. We did not predetermine sample sizes, but our sample sizes are similar to those generally employed in the field.

AUTHOR INFORMATION

Corresponding Authors

Tongyu Zhu − *Department of Urology, Zhongshan Hospital Fudan University, Shanghai 200030, China; Shanghai Key Laboratory of Organ Transplantation, Shanghai 200030, China;* orcid.org/0009-0001-2391-4628; Phone: 021-64041990; Email: drtongyuzhu@yeah.net

Guoyi Wu − *Shanghai Public Health Clinical Center, Fudan University, Shanghai 201500, China*; Phone: 021-37990333; Email: wuguoyi@163.com

Authors

Zhiyu Qian − *Department of Urology, Zhongshan Hospital Fudan University, Shanghai 200030, China; Shanghai Key Laboratory of Organ Transplantation, Shanghai 200030, China*

Xinyue Zhang − *Shanghai Skin Disease Hospital, School of Medicine, Tongji University, Shanghai 200443, China*

Jiahua Huang − *Shanghai Public Health Clinical Center, Fudan University, Shanghai 201500, China*

Xinhao Niu − *Department of Urology, Zhongshan Hospital Fudan University, Shanghai 200030, China; Shanghai Key Laboratory of Organ Transplantation, Shanghai 200030, China*

Cuisong Zhu − *Shanghai Public Health Clinical Center, Fudan University, Shanghai 201500, China*

Zongguang Tai − *Shanghai Skin Disease Hospital, School of Medicine, Tongji University, Shanghai 200443, China*

Quangang Zhu − *Shanghai Skin Disease Hospital, School of Medicine, Tongji University, Shanghai 200443, China*

Zhongjian Chen − *Shanghai Skin Disease Hospital, School of Medicine, Tongji University, Shanghai 200443, China*

Complete contact information is available at: https://pubs.acs.org/10.1021/acsomega.4c01624

Author Contributions

⊥Z.Q. and X.Z. contributed equally to this work.

Notes

The authors declare no competing financial interest.

ACKNOWLEDGMENTS

We are grateful for the help of Lifei Liang and Yufeng Zhao of Zhongshan Hospital. This work was supported by the Shanghai Municipal Key Clinical Specialty (no. shslczdzk05802), the Jinshan Science and Technology Committee (no. 2020-3-64), and the Shanghai Science and Technology Committee Science and Technology Innovation Program (no. 21S11902600).

ABBREVIATIONS

ALT, alanine aminotransferase; AST, aspartate transaminase; BCA, bicinchoninic acid; BUN, blood urea nitrogen; CCK-8, cell counting kit-8; DAPI, 4,6-diamidino-2-phenylindole; DMEM, Dulbecco's modified Eagle medium; DMSO, dimethyl sulfoxide; DSPE, distearoyl-*sn*-glycero-3-phosphoethanolamine; ELISA, enzyme-linked immunosorbent assay; EM, exosome mimetics; GPx4, glutathione peroxidase-4; GSH, glutathione; GSSG, glutathione disulfide; HE, hematoxylin−eosin; IHC, immunohistochemistry; IL, interleukin; IR, ischemia−reperfusion; MDA, malonaldehyde; MHY1485, 4,6-dimorpholino-*N*-(4-nitrophenyl)-1,3,5-triazin-2-amine; MSC, mesenchymal stromal/stem cell; MT-EM, MSC-TK exosome mimetics; MTM-EM, MSC-TK-MHY1485 exosome mimetics; mTOR, mammalian target of rapamycin; mTORC1, mammalian target of rapamycin complex 1; PAS, periodic acid-Schiff; OD, optical density; PBS, phosphate buffer solution; PDI, polymer dispersity index; PEG, polyethylene glycol; PMSC, placenta mesenchymal stromal/stem cell; PI, propidium iodide; ROS, reactive oxygen species; SOD, superoxide dismutase; Scr, serum creatinine; TCMK-1, transformed C3H mouse kidney-1; TEM, transmission electron microscope; TK, thioketal; TNF, tumor necrosis factor; uIRIx, unilateral IRI with contralateral nephrectomy

REFERENCES

(1) Malek, M.; Nematbakhsh, M. Renal ischemia/reperfusion injury; from pathophysiology to treatment. *J. Renal Inj. Prev.* **2015**, *4* (2), 20−27.

(2) Shiva, N.; Sharma, N.; Kulkarni, Y. A.; Mulay, S. R.; Gaikwad, A. B. Renal ischemia/reperfusion injury: An insight on in vitro and in vivo models. *Life Sci.* **2020**, *256*, 117860.

(3) Fan, H.; Liu, J.; Sun, J.; Feng, G.; Li, J. Advances in the study of B cells in renal ischemia-reperfusion injury. *Front. Immunol.* **2023**, *14*, 1216094.

(4) Chen, D. Q.; Guo, Y.; Li, X.; Zhang, G. Q.; Li, P. Small molecules as modulators of regulated cell death against ischemia/reperfusion injury. *Med. Res. Rev.* **2022**, *42* (6), 2067−2101.

(5) Hosohata, K.; Harnsirikarn, T.; Chokesuwattanaskul, S. Ferroptosis: A Potential Therapeutic Target in Acute Kidney Injury. *Int. J. Mol. Sci.* **2022**, *23* (12), 6583.

(6) Nieuwenhuijs-Moeke, G. J.; Pischke, S. E.; Berger, S. P.; Sanders, J. S. F.; Pol, R. A.; Struys, M.; Ploeg, R. J.; Leuvenink, H. G. D. Ischemia and Reperfusion Injury in Kidney Transplantation: Relevant Mechanisms in Injury and Repair. *J. Clin. Med.* **2020**, *9* (1), 253.

(7) Nguyen, Q. T. T.; Hoang, T. X.; Ryu, H.; Oh, K. H.; Kim, J. Y. Synergistic Antiproliferative Effects of All-Trans Retinoic Acid and Paclitaxel on Autosomal Dominant Polycystic Kidney Disease Epithelial Cells. *BioMed Res. Int.* **2021**, *2021*, 1−12.
(8) Chen, W. R.; Liu, H. B.; Chen, Y. D.; Sha, Y.; Ma, Q.; Zhu, P. J.; Mu, Y. Melatonin Attenuates Myocardial Ischemia/Reperfusion Injury by Inhibiting Autophagy Via an AMPK/mTOR Signaling Pathway. *Cell. Physiol. Biochem.* **2018**, *47* (5), 2067−2076.
(9) Fang, X.; Zhang, J.; Li, Y.; Song, Y.; Yu, Y.; Cai, Z.; Lian, F.; Yang, J.; Min, J.; Wang, F. Malic Enzyme 1 as a Novel Anti-Ferroptotic Regulator in Hepatic Ischemia/Reperfusion Injury. *Adv. Sci.* **2023**, *10* (13), No. e2205436.
(10) Bei, Y.; Lu, D.; Bar, C.; Chatterjee, S.; Costa, A.; Riedel, I.; Mooren, F. C.; Zhu, Y.; Huang, Z.; Wei, M.; Hu, M.; Liu, S.; Yu, P.; Wang, K.; Thum, T.; Xiao, J. miR-486 attenuates cardiac ischemia/reperfusion injury and mediates the beneficial effect of exercise for myocardial protection. *Mol. Ther.* **2022**, *30* (4), 1675−1691.
(11) Zhang, R.; Liu, Y.; You, J.; Ge, B. Tanshinone IIA inhibits ischemia-reperfusion-induced inflammation, ferroptosis and apoptosis through activation of the PI3K/Akt/mTOR pathway. *Hum. Exp. Toxicol.* **2023**, *42*, 9603271231180864.
(12) Loewith, R.; Jacinto, E.; Wullschleger, S.; Lorberg, A.; Crespo, J. L.; Bonenfant, D.; Oppliger, W.; Jenoe, P.; Hall, M. N. Two TOR complexes, only one of which is rapamycin sensitive, have distinct roles in cell growth control. *Mol. Cell* **2002**, *10* (3), 457−468.
(13) Laplante, M.; Sabatini, D. M. mTOR signaling in growth control and disease. *Cell* **2012**, *149* (2), 274−293.
(14) Villa-Gonzalez, M.; Martin-Lopez, G.; Perez-Alvarez, M. J. Dysregulation of mTOR Signaling after Brain Ischemia. *Int. J. Mol. Sci.* **2022**, *23* (5), 2814.
(15) Yang, H.; Wen, Y.; Zhang, M.; Liu, Q.; Zhang, H.; Zhang, J.; Lu, L.; Ye, T.; Bai, X.; Xiao, G.; Wang, M. MTORC1 coordinates the autophagy and apoptosis signaling in articular chondrocytes in osteoarthritic temporomandibular joint. *Autophagy* **2020**, *16* (2), 271−288.
(16) Kholodenko, I. V.; Kholodenko, R. V.; Yarygin, K. N. The Crosstalk between Mesenchymal Stromal/Stem Cells and Hepatocytes in Homeostasis and under Stress. *Int. J. Mol. Sci.* **2023**, *24* (20), 15212.
(17) Miceli, V.; Bulati, M.; Gallo, A.; Iannolo, G.; Busa, R.; Conaldi, P. G.; Zito, G. Role of Mesenchymal Stem/Stromal Cells in Modulating Ischemia/Reperfusion Injury: Current State of the Art and Future Perspectives. *Biomedicines* **2023**, *11* (3), 689.
(18) Wu, X. D.; Kang, L.; Tian, J.; Wu, Y.; Huang, Y.; Liu, J.; Wang, H.; Qiu, G.; Wu, Z. Exosomes derived from magnetically actuated bone mesenchymal stem cells promote tendon-bone healing through the miR-21−5p/SMAD7 pathway. *Mater. Today Bio* **2022**, *15*, 100319.
(19) Marks, P. W.; Witten, C. M.; Califf, R. M. Clarifying Stem-Cell Therapy's Benefits and Risks. *N. Engl. J. Med.* **2017**, *376* (11), 1007−1009.
(20) Xue, Y.; Riva, N.; Zhao, L.; Shieh, J. S.; Chin, Y. T.; Gatt, A.; Guo, J. J. Recent advances of exosomes in soft tissue injuries in sports medicine: A critical review on biological and biomaterial applications. *J. Controlled Release* **2023**, *364*, 90−108.
(21) Rao, D.; Huang, D.; Sang, C.; Zhong, T.; Zhang, Z.; Tang, Z. Advances in Mesenchymal Stem Cell-Derived Exosomes as Drug Delivery Vehicles. *Front. Bioeng. Biotechnol.* **2022**, *9*, 797359.
(22) Shao, H.; Im, H.; Castro, C. M.; Breakefield, X.; Weissleder, R.; Lee, H. New Technologies for Analysis of Extracellular Vesicles. *Chem. Rev.* **2018**, *118* (4), 1917−1950.
(23) Rani, S.; Ritter, T. The Exosome - A Naturally Secreted Nanoparticle and its Application to Wound Healing. *Adv. Mater.* **2016**, *28* (27), 5542−5552.
(24) Lindenbergh, M. F. S.; Stoorvogel, W. Antigen Presentation by Extracellular Vesicles from Professional Antigen-Presenting Cells. *Annu. Rev. Immunol.* **2018**, *36*, 435−459.
(25) Piko, N.; Bevc, S.; Hojs, R.; Ekart, R. The Role of Oxidative Stress in Kidney Injury. *Antioxidants* **2023**, *12* (9), 1772.
(26) Hao, P.; Wu, X.; Wang, L.; Wei, S.; Xu, H.; Huang, W.; Li, Y.; Zhang, T.; Zan, X. One-Pot Generating Subunit Vaccine with High Encapsulating Efficiency and Fast Lysosome Escape for Potent Cellular Immune Response. *Bioconjugate Chem.* **2020**, *31* (8), 1917−1927.
(27) Van de Vyver, T.; Bogaert, B.; De Backer, L.; Joris, F.; Guagliardo, R.; Van Hoeck, J.; Merckx, P.; Van Calenbergh, S.; Ramishetti, S.; Peer, D.; Remaut, K.; De Smedt, S. C.; Raemdonck, K. Cationic Amphiphilic Drugs Boost the Lysosomal Escape of Small Nucleic Acid Therapeutics in a Nanocarrier-Dependent Manner. *ACS Nano* **2020**, *14* (4), 4774−4791.
(28) Zhao, X.; Li, Y.; Wu, S.; Wang, Y.; Liu, B.; Zhou, H.; Li, F. Role of extracellular vesicles in pathogenesis and therapy of renal ischemia-reperfusion injury. *Biomed. Pharmacother.* **2023**, *165*, 115229.
(29) Williams, T. M.; Wise, A. F.; Layton, D. S.; Ricardo, S. D. Phenotype and influx kinetics of leukocytes and inflammatory cytokine production in kidney ischemia/reperfusion injury. *Nephrology* **2018**, *23* (1), 75−85.
(30) Crorkin, P.; Hao, S.; Ferreri, N. R. Responses to Ang II (Angiotensin II), Salt Intake, and Lipopolysaccharide Reveal the Diverse Actions of TNF-α (Tumor Necrosis Factor-α) on Blood Pressure and Renal Function. *Hypertension* **2022**, *79* (12), 2656−2670.
(31) Li, Y.; Zhao, J.; Yin, Y.; Li, K.; Zhang, C.; Zheng, Y. The Role of IL-6 in Fibrotic Diseases: Molecular and Cellular Mechanisms. *Int. J. Biol. Sci.* **2022**, *18* (14), 5405−5414.
(32) Sfakianos, A. P.; Mellor, L. E.; Pang, Y. F.; Kritsiligkou, P.; Needs, H.; Abou-Hamdan, H.; Desaubry, L.; Poulin, G. B.; Ashe, M. P.; Whitmarsh, A. J. The mTOR-S6 kinase pathway promotes stress granule assembly. *Cell Death Differ.* **2018**, *25* (10), 1766−1780.
(33) Xu, J.; Li, X.; Yuan, Q.; Wang, C.; Xu, L.; Wei, X.; Liu, H.; Yu, B.; An, Z.; Zhao, Y.; Li, X.; Zhang, X.; Ma, X.; Cai, M. The semaphorin 4A-neuropilin 1 axis alleviates kidney ischemia reperfusion injury by promoting the stability and function of regulatory T cells. *Kidney Int.* **2021**, *100* (6), 1268−1281.
(34) Zhang, X. D.; Liu, Z. Y.; Wang, M. S.; Guo, Y. X.; Wang, X. K.; Luo, K.; Huang, S.; Li, R. F. Mechanisms and regulations of ferroptosis. *Front. Immunol.* **2023**, *14*, 1269451.
(35) Sun, K.; Zhi, Y.; Ren, W.; Li, S.; Zhou, X.; Gao, L.; Zhi, K. The mitochondrial regulation in ferroptosis signaling pathway and its potential strategies for cancer. *Biomed. Pharmacother.* **2023**, *169*, 115892.
(36) Fujii, J.; Homma, T.; Osaki, T. Superoxide Radicals in the Execution of Cell Death. *Antioxidants* **2022**, *11* (3), 501.
(37) Hu, X.; Bao, Y.; Li, M.; Zhang, W.; Chen, C. The role of ferroptosis and its mechanism in ischemic stroke. *Exp. Neurol.* **2024**, *372*, 114630.
(38) Jones, D. P. Redefining oxidative stress. *Antioxid. Redox Signaling* **2006**, *8* (9−10), 1865−1879.
(39) Moldogazieva, N. T.; Zavadskiy, S. P.; Astakhov, D. V.; Terentiev, A. A. Lipid peroxidation: Reactive carbonyl species, protein/DNA adducts, and signaling switches in oxidative stress and cancer. *Biochem. Biophys. Res. Commun.* **2023**, *687*, 149167.
(40) Li, Z.; Lange, M.; Dixon, S. J.; Olzmann, J. A. Lipid Quality Control and Ferroptosis: From Concept to Mechanism. *Annu. Rev. Biochem.* **2023**, *93*, 1.1.
(41) Shi, Y.; Wang, Y.; Li, Q.; Liu, K.; Hou, J.; Shao, C.; Wang, Y. Immunoregulatory mechanisms of mesenchymal stem and stromal cells in inflammatory diseases. *Nat. Rev. Nephrol.* **2018**, *14* (8), 493−507.
(42) Deng, Z.; He, M.; Hu, H.; Zhang, W.; Zhang, Y.; Ge, Y.; Ma, T.; Wu, J.; Li, L.; Sun, M.; An, S.; Li, J.; Huang, Q.; Gong, S.; Zhang, J.; Chen, Z.; Zeng, Z. Melatonin attenuates sepsis-induced acute kidney injury by promoting mitophagy through SIRT3-mediated TFAM deacetylation. *Autophagy* **2023**, *20*, 151−165.
(43) Nagata, S.; Segawa, K. Sensing and clearance of apoptotic cells. *Curr. Opin. Immunol.* **2021**, *68*, 1−8.

https://doi.org/10.1021/acsomega.4c01624
ACS Omega 2024, 9, 24853−24863

(44) Li, S.; Zhang, W.; Hu, X. Comprehensive analysis of necroptosis-related genes in renal ischemia-reperfusion injury. *Front. Immunol.* **2023**, *14*, 1279603.
(45) Zhou, T.; Yuan, Z.; Weng, J.; Pei, D.; Du, X.; He, C.; Lai, P. Challenges and advances in clinical applications of mesenchymal stromal cells. *J. Hematol. Oncol.* **2021**, *14* (1), 24.
(46) Elahi, F. M.; Farwell, D. G.; Nolta, J. A.; Anderson, J. D. Preclinical translation of exosomes derived from mesenchymal stem/stromal cells. *Stem Cell.* **2020**, *38* (1), 15−21.
(47) Yin, K.; Wang, S.; Zhao, R. C. Exosomes from mesenchymal stem/stromal cells: a new therapeutic paradigm. *Biomark. Res.* **2019**, *7*, 8.
(48) O'Brien, K.; Breyne, K.; Ughetto, S.; Laurent, L. C.; Breakefield, X. O. RNA delivery by extracellular vesicles in mammalian cells and its applications. *Nat. Rev. Mol. Cell Biol.* **2020**, *21* (10), 585−606.
(49) Kalogeris, T.; Baines, C. P.; Krenz, M.; Korthuis, R. J. Cell biology of ischemia/reperfusion injury. *Int. Rev. Cell Mol. Biol.* **2012**, *298*, 229−317.
(50) Zhang, B.; Chen, Z. Y.; Jiang, Z.; Huang, S.; Liu, X. H.; Wang, L. Nephroprotective Effects of Cardamonin on Renal Ischemia Reperfusion Injury/UUO-Induced Renal Fibrosis. *J. Agric. Food Chem.* **2023**, *71* (36), 13284−13303.
(51) Zhang, J.; He, W.; Zheng, D.; He, Q.; Tan, M.; Jin, J. Exosomal-miR-1184 derived from mesenchymal stem cells alleviates cisplatin-associated acute kidney injury. *Mol. Med. Rep.* **2021**, *24* (5), 795.
(52) Zhang, R.; Zhu, Y.; Li, Y.; Liu, W.; Yin, L.; Yin, S.; Ji, C.; Hu, Y.; Wang, Q.; Zhou, X.; Chen, J.; Xu, W.; Qian, H. Human umbilical cord mesenchymal stem cell exosomes alleviate sepsis-associated acute kidney injury via regulating microRNA-146b expression. *Biotechnol. Lett.* **2020**, *42* (4), 669−679.
(53) Cao, S.; Huang, Y.; Dai, Z.; Liao, Y.; Zhang, J.; Wang, L.; Hao, Z.; Wang, F.; Wang, D.; Liu, L. Circular RNA mmu_circ_0001295 from hypoxia pretreated adipose-derived mesenchymal stem cells (ADSCs) exosomes improves outcomes and inhibits sepsis-induced renal injury in a mouse model of sepsis. *Bioengineered* **2022**, *13* (3), 6323−6331.
(54) Whelan, R. S.; Kaplinskiy, V.; Kitsis, R. N. Cell death in the pathogenesis of heart disease: mechanisms and significance. *Annu. Rev. Physiol.* **2010**, *72*, 19−44.
(55) Zhu, G.; Pei, L.; Lin, F.; Yin, H.; Li, X.; He, W.; Liu, N.; Gou, X. Exosomes from human-bone-marrow-derived mesenchymal stem cells protect against renal ischemia/reperfusion injury via transferring miR-199a-3p. *J. Cell. Physiol.* **2019**, *234* (12), 23736−23749.
(56) Wang, C.; Zhu, G.; He, W.; Yin, H.; Lin, F.; Gou, X.; Li, X. BMSCs protect against renal ischemia-reperfusion injury by secreting exosomes loaded with miR-199a-5p that target BIP to inhibit endoplasmic reticulum stress at the very early reperfusion stages. *FASEB J.* **2019**, *33* (4), 5440−5456.
(57) Han, J.; Wang, L.; Lv, H.; Liu, J.; Dong, Y.; Shi, L.; Ji, Q. EphA2 inhibits SRA01/04 cells apoptosis by suppressing autophagy via activating PI3K/Akt/mTOR pathway. *Arch. Biochem. Biophys.* **2021**, *711*, 109024.
(58) Dixon, S. J.; Lemberg, K. M.; Lamprecht, M. R.; Skouta, R.; Zaitsev, E. M.; Gleason, C. E.; Patel, D. N.; Bauer, A. J.; Cantley, A. M.; Yang, W. S.; Morrison, B.; Stockwell, B. R. Ferroptosis: an iron-dependent form of nonapoptotic cell death. *Cell* **2012**, *149* (5), 1060−1072.
(59) Su, L.; Jiang, X.; Yang, C.; Zhang, J.; Chen, B.; Li, Y.; Yao, S.; Xie, Q.; Gomez, H.; Murugan, R.; Peng, Z. Pannexin 1 mediates ferroptosis that contributes to renal ischemia/reperfusion injury. *J. Biol. Chem.* **2019**, *294* (50), 19395−19404.
(60) Zweier, J. L.; Flaherty, J. T.; Weisfeldt, M. L. Direct measurement of free radical generation following reperfusion of ischemic myocardium. *Proc. Natl. Acad. Sci. U.S.A.* **1987**, *84* (5), 1404−1407.
(61) Cao, J. Y.; Wang, B.; Tang, T. T.; Wen, Y.; Li, Z. L.; Feng, S. T.; Wu, M.; Liu, D.; Yin, D.; Ma, K. L.; Tang, R. N.; Wu, Q. L.; Lan, H. Y.; Lv, L. L.; Liu, B. C. Exosomal miR-125b-5p deriving from mesenchymal stem cells promotes tubular repair by suppression of p53 in ischemic acute kidney injury. *Theranostics* **2021**, *11* (11), 5248−5266.
(62) Tan, X.; Tao, Q.; Yin, S.; Fu, G.; Wang, C.; Xiang, F.; Hu, H.; Zhang, S.; Wang, Z.; Li, D. A single administration of FGF2 after renal ischemia-reperfusion injury alleviates post-injury interstitial fibrosis. *Nephrol. Dial. Transplant.* **2023**, *38* (11), 2537−2549.

https://doi.org/10.1021/acsomega.4c01624
ACS Omega 2024, 9, 24853−24863